

Systematic studies of SiGe/Si islands nucleated via separate *in situ* or *ex situ* Ga⁺ focused ion beam-guided growth techniques

Thomas E. Vandervelde

Department of Physics, University of Virginia, 382 McCormick Road, Charlottesville, Virginia 22904

Surajit Atha and Robert Hull

Department of Materials Science, University of Virginia, 116 Engineers Way, Charlottesville, Virginia 22904

Timothy L. Pernell and John C. Bean^{a)}

Department of Electrical and Computer Engineering, University of Virginia, 351 McCormick Road, Charlottesville, Virginia 22904

(Received 13 September 2005; accepted 17 January 2006; published 27 February 2006)

In this study, we use 25 keV *in situ* and 30 keV *ex situ* Ga⁺ focused ion beams (FIBs) to locally modify the substrate before deposition and determine their effects on nucleation of molecular beam epitaxy grown Ge/Si islands. FIB processing may alter island formation in at least five ways: the surfactant effect of Ga⁺, doping effects of subsurface Ga⁺, local strains, crystalline damage, and surface roughening. To explore these possibilities, we milled square regions of increasing Ga⁺ doses and used atomic force microscopy to monitor islanding in and around these regions. For *in situ* experiments, doses ranged from $\sim 10^{13}$ to 5×10^{17} ions/cm² (0.04–400 ML). We began to observe changes in island topology at doses as low as $\sim 10^{14}$ ions/cm². For doses of $\sim 10^{15}$ to $\sim 8 \times 10^{16}$ ions/cm² (2–160 ML), implanted areas were surrounded by denuded zones that grew from ~ 0.5 to $6 \mu\text{m}$ with increasing dose. Immediately inside the implanted area, island size and concentration appeared to peak. At doses above $\sim 6 \times 10^{16}$ ions/cm² (120 ML), Ga⁺ produced noticeable surface depressions, which were often surrounded by enhanced island densities, rather than a denuded zone. For *ex situ* FIB patterning, samples underwent both pregrowth cleaning and growth of a thin capping layer (0–100 nm). Doses ranging from 7.5×10^{13} to $\sim 10^{17}$ ions/cm² (0.15–200 ML) were used in concert with varied capping layer thicknesses to study their combined affect on island nucleation. The results correspond well with *in situ* experiments for thin capping layers. Increased capping layer thickness resulted in muted modifications to island formation for low Ga⁺ doses, while for higher doses trends similar to those obtained *in situ* are seen. © 2006 American Vacuum Society. [DOI: 10.1116/1.2172952]

I. BACKGROUND

Epitaxial growth of SiGe over Si (001) has been extensively studied.^{1–14} This system is known to follow the Stranski-Krastanov mode of growth, with 60° misfit dislocations and three dimensional (3D) islanding playing critical roles in relieving the strain energy that builds up due to the lattice mismatch between the substrate and the film. The different stages of islanding include the formation of pyramidal hut clusters with <501> facets, followed by the formation of larger dome islands with primarily [201] and [311] facets, and finally enlargement of the domes through introduction of misfit dislocation. Several groups have studied the transition between the different stages of island growth. Floro *et al.* recently showed that the strain-driven roughening behavior in low mismatch (low x for Si_{1-x}Ge_x) cases is qualitatively the same as that at much higher strains, including the 4.2% mismatch of Ge on Si (001).¹¹ Ross *et al.* has characterized the transition of hut cluster to dome morphology with specific reference to growth of Ge over Si (001).¹⁴ It has been shown, both by experimental observations and simulation,

that some of the hut clusters continue to grow, change shape, and become domes, whereas others reduce in size and disappear. Thus, over a growth period, a bimodal size distribution is observed where both hut clusters and domes of distinctly different sizes and shapes can be seen. Ultimately, a steady state is reached where domes reach a size plateau, beyond which growth is not possible without dislocations. Ross *et al.* also suggested that their model might extend from the transition of strained coherent domes to even larger dislocated islands. The transition should be similar to the hut-to-dome transition in that, after the domes reach their size plateau, some dislocate and grow in size at the cost of the others, which shrink and disappear, similar to that of the hut clusters.¹⁵

Island formation and growth of epitaxial SiGe/Si (001) films are governed by both thermodynamic and kinetic factors; parameters such as growth rate, growth temperature, and Ge fraction play important roles. Many researchers have tried to modify the nucleation and growth of islands using surface lithography and surfactant effects.^{16–23} Several surfactants, including Sn, Sb, Bi, and B, control island formation by affecting their size and number density. Wakayama

^{a)}Electronic mail: jcb6t@virginia.edu

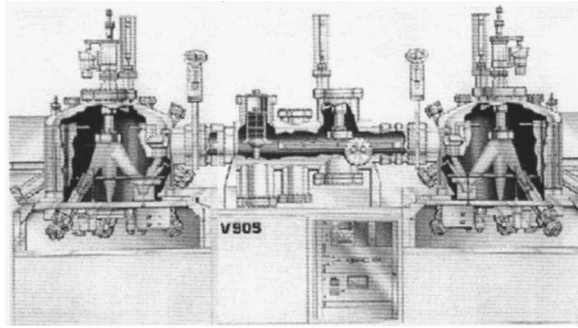


FIG. 1. Dual VG 90s MBE system used in these experiments. The main deposition chamber is on the far right and the FIB is installed in the preparation chamber near its center.

et al. demonstrated a multistep procedure that introduced a submonolayer C deposition step to control the structure, size, and density of Ge dots on Si (001).²⁴

In this work, we guide the nucleation of islands by modification of the Si (001) surface using *ex situ* or *in situ* Ga⁺ focused ion beams. Exploring the *ex situ* technique is important because most fabrication facilities may not be able to integrate an *in situ* focused ion beam (FIB) into their production line. The FIB allows us to modify the substrate in three distinct ways: morphologically, surface damage and amorphization, and chemical effect. Often these three phenomena are interrelated, thus separating the effects poses a challenge. A previously published work by Kammler *et al.* demonstrated the ability to control the formation of Ge dots using an *in situ* FIB.²⁵ Their work, however, relied on the use of chemical vapor deposition, which fundamentally differs from molecular beam epitaxy (MBE)-based techniques we employ. We explored the dose-dependent effects of milling a Si Substrate with a Ga⁺ FIB column upon subsequent Ge nucleation. Additionally, we determined the robustness of this technique to subsequent burial by a variable thickness Si capping layer deposited upon the as-prepatterned and cleaned surface.

II. EXPERIMENT

A. Instrumentation

Here, we used two separate FEI company FIB columns to modify the substrate: an *in situ* FIB, incorporated into the MBE system, and an *ex situ* FIB. The two FIBs are nearly identical in configuration but there are a few differences. The *in situ* FIB is a FEI model that uses two octupole lenses to collimate and a fixed aperture to focus the beam and truncate beam current from 1 pA to ~8 nA. This model has a maximum accelerating voltage of 25 keV, minimum beam size of ~20 nm, and a maximum field of view of ~1 mm². The *ex situ* FIB is a FEI 200 model, which works with an accelerating voltage of 30 keV. Different beam currents can be selected by an automatic variable aperture strip with a range of 1 pA to 11.5 nA. The minimum beam diameter for this FIB column is ~10 nm, using a 1 pA beam current. The field of view in both FIBs is divided into an array of 1024

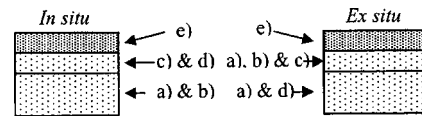


FIG. 2. Schematic of the experimental process with order of occurrence progressing from bottom to top. (a) P clean, (b) *in situ* anneal, (c) Si deposition, (d) FIB patterning, and (e) Ge deposition.

× 1024 individually addressable pixels, thus allowing for precise control of the region to be modified.

Our laboratory is equipped with a unique and highly capable dual-growth chamber MBE system (Fig. 1). The right chamber of this system is intended for *e*-gun-based growth of SiGe. Wafers as large as 150 mm diameter may be used. The base pressure in the chamber prior to growth was typically 2×10^{-10} Torr. The *in situ* FIB is located in the central preparation chamber to prevent any deposition from damaging the column. The FIB and its sample stage are mounted on a bellows-isolated flange that is bolted to the laboratory floor, making it largely immune to the MBE system's cryopump vibrations.

Growth results were characterized through the use of *ex situ* tapping mode atomic force microscopy (AFM). This microscopy was done using a Digital Instruments' Dimension 3100 Nanoscope AFM.

B. Methods

The purpose of this work was to investigate the effect of increasing Ga⁺ implantation and sputtering on the Ge nucleation process. This was investigated using the *in situ* FIB. In addition, with an *ex situ* FIB we explored how capping of the sputtered region in a Si buffer layer affects these results. This is important because most fabrication facilities may not be able to integrate an *in situ* FIB into their production line. Additionally, burial of layers is often required for technological applications.

For *in situ* FIB-based experiments, a matrix of nine $10 \times 10 \mu\text{m}^2$ squares, with incrementally increasing doses of Ga⁺, were implanted; doses ranged from $\sim 10^{13}$ to $\sim 10^{18}$ ions/cm² (0.1–2000 ML). Recall that for Si, a single atomic monolayer is $\sim 5 \times 10^{14}$ atoms/cm². Throughout this procedure, the deposition chamber had a base pressure of 2×10^{-10} Torr, with FIB irradiation occurring at a base pressure of 1×10^{-9} Torr in the preparation chamber. This means that the sample never left UHV and therefore gathers minimal contaminants. After FIB exposure, 10 ML of Ge were grown at 750 °C and a rate of 0.4 Å/s, which led to the formation of islands. Figure 2 details this sequence.

Ex situ fabrications were performed under HV conditions (10^{-6} Torr range). The FIB was used to pattern eight separate $5 \times 5 \mu\text{m}^2$ areas with increasing doses of Ga⁺, ranging from 7.5×10^{13} to 1.05×10^{17} ions/cm² (0.15–210 ML). Figure 3 shows AFM images of regions following *ex situ* FIB fabrication. Prior to loading into the MBE, these samples were first cleaned using a modified piranha procedure that leaves the samples H terminated. Once in the system, but prior to

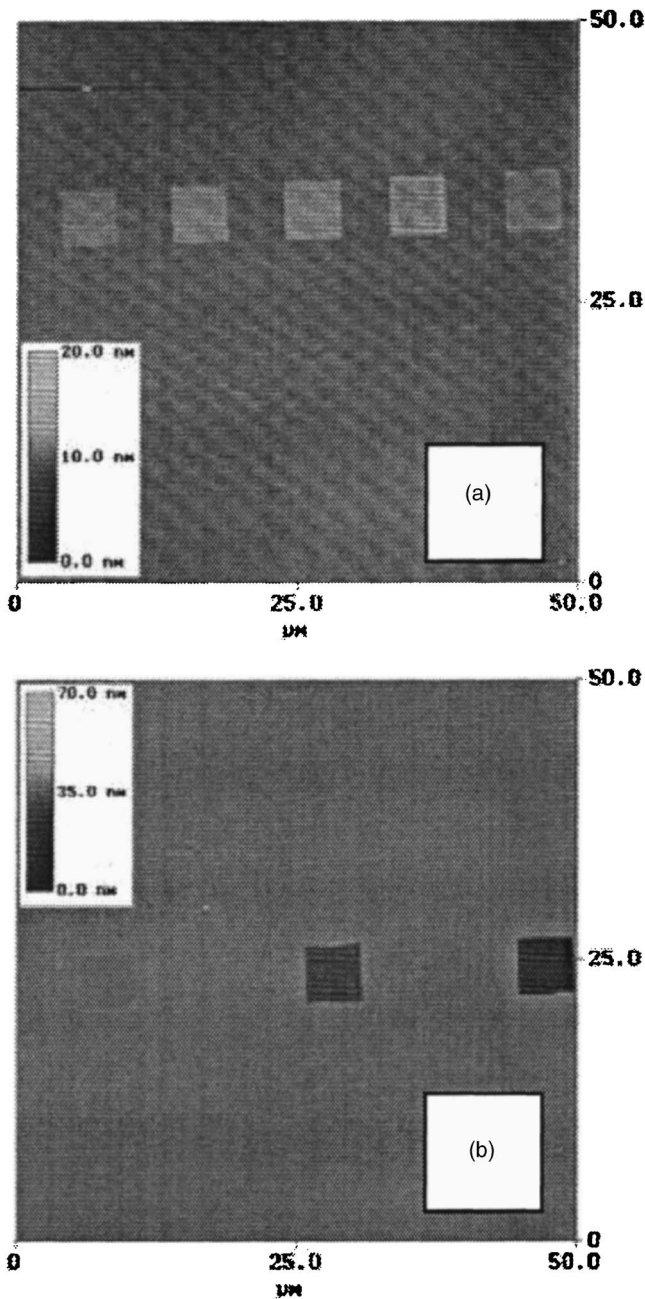


FIG. 3. AFM images of FIB modified regions prior to MBE growth show. (A) Topological effects of low-dose FIB patterning. AFM image (section analysis mode) showing five $5 \times 5 \mu\text{m}^2$ regions implanted with low doses of Ga, 7.5×10^{13} , 1.5×10^{14} , 2.75×10^{14} , 8.25×10^{14} , and 3.57×10^{15} ions/cm² or 0.15, 0.3, 0.55, 1.65, and 7.14 ML (left to right). These low-dose fabrications generate a raised area, 1–2 nm in height. (B) Topological effects of high-dose FIB patterning. AFM image (section analysis mode) showing $5 \times 5 \mu\text{m}^2$ regions implanted with the three highest doses of Ga, 8.75×10^{15} , 3.5×10^{16} , and 1.05×10^{17} ions/cm² or 17.5, 70, and 210 ML (left to right). High doses of Ga generate depressions that deepen proportionally with Ga concentration.

Ge deposition, the samples were heated and capped with Si (Fig. 2).

AFM imaging of our *ex situ* samples, prior to deposition, showed that lower doses of Ga during FIB patterning led to surface swelling, with height increases ranging from 1 to 2

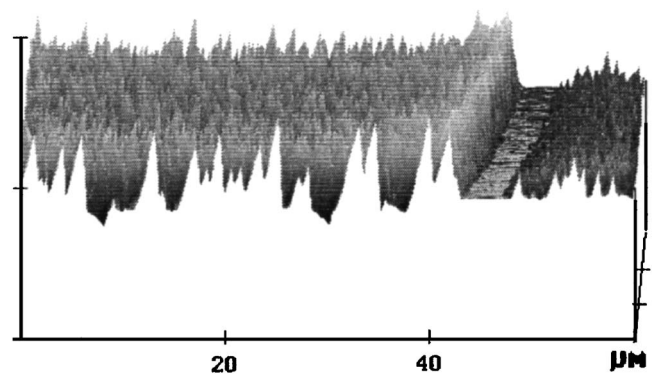


FIG. 4. Effect of Ga implantation with subsequent Ge deposition analyzed by AFM. Increased island height and number density in the implanted region ($\sim 10^{15}$ ions/cm² or 1 ML, left). Normal island growth, separated by a few micron wide denuded zone, in the untreated region (right).

nm (Fig. 3). This may result because the incident ions have sufficient flux to disrupt some of the crystalline bonds of Si, amorphizing it, which increases its volume.^{26,27} At increasingly higher doses, more sputtering occurs and surface depressions of increasing depth are created. This leads to the formation of depressions with observed depths of ~ 30 nm for Ga at the highest dose, 1.05×10^{17} ions/cm² (210 ML). Although sputtering occurs for any Ga dose, pit formation due to sputtering is initially masked by the increase in height due to the amorphization of the lattice.

III. RESULTS

A. *In situ* without Si capping layer

In order to study the effect of Ga dose on Ge island nucleation, we studied samples with Ga FIB implant doses ranging from 2×10^{13} to 2×10^{17} ions/cm² (0.04–400 ML), which were then overgrown with 10 ML of Ge. Figure 4 illustrates the drastic effect of Ga⁺ on island morphology, particularly at the boundary between a region that had been treated with Ga (located within the range of 0 to $\sim 42 \mu\text{m}$ in Fig. 4) and one that received no Ga at all (located within the range of $\sim 42 \mu\text{m}$ and up in the figure). This transition is characteristic of our results. Regions treated with Ga⁺ have a higher island-number density and tend to form taller islands when compared with unmodified regions. In the untreated region, near the boundary between it and the Ga-implanted area, a denuded zone of a few microns in width, was observed. This may imply that the FIB is altering the surface in two ways, topologically and via a surfactant effect, as discussed below. First, the patterned area acts as a preferential attachment site due to the topological changes caused by the FIB. Second, the appearance of a large denuded zone beyond the patterned region suggests that the Ga is active as a surfactant on the surface. Some surfactants, such as Ga for the Si/Ge system, increase the diffusion length of the adatoms allowing them to sample a greater area for a preferential attachment site. This increased mobility, when in the presence of a highly preferential attachment site, allows for the

formation of a large denuded zone. This is further confirmed by the Ga dose-dependant size of the denuded zone, discussed below.

When combined into a matrix of nine increasing doses, additional effects of Ga⁺ on island nucleation were observed [Figs. 5(a) and 5(b)]. In the first square [Fig. 5(a), region No. 1], which is visually missing from the pattern, the Ga dose of 2×10^{13} ions/cm² (0.04 ML) did not appear to alter the local island distribution. Effects began to appear, however, with higher doses. In the second square [Fig. 5(a), region No. 2], a dose of $\sim 10^{14}$ ions/cm² (0.2 ML) led to the appearance of a denuded zone, along with increased island-number density, at the interface between the area modified by the FIB and the rest of the sample.

A magnified view of a denuded zone of region No. 1 (Ga⁺ dose of 2×10^{13} ions/cm²) is shown in Fig. 5(c). This shows that for even extremely low Ga doses Ge nucleation is affected. The intermediate squares, with doses ranging from 5×10^{14} to 5×10^{15} ions/cm² (1–10 ML) [Fig. 5(a), region Nos. 3–5], demonstrated continued expansion of the denuded zone and increases in island-number density, especially at the edges of the modified region. At a higher dose of $\sim 10^{16}$ ions/cm² (20 ML), topography begins to develop [Fig. 5(a), region No. 6], which is observed as a deepening central depression in the milled region. Continued deepening of this pit resulted in shrinkage of the denuded zone and a disappearance of islanding in the milled region when treated with successively increasing doses [Fig. 5(a), region Nos. 7–9].

This indicates that the denuded zone is formed due to a mass transfer. Essentially, the implanted region is a site of preferential attachment for incoming adatoms. Thus, nearby adatoms enter this region through surface diffusion and stick, creating an area devoid of material outside its borders. The longer the diffusion length of the adatoms, the larger the denuded zone formed, barring a significant barrier to diffusion (e.g., an Erlich-Schwoebel barrier). As the Ga dose increases, the diffusion length increases and, correspondingly, so does the size of the denuded zone. At high doses, significant milling occurs, forming a central depression separating the implanted region from the rest of the surface by steep cliffs. Cliff edges deter the transfer of material, thereby cutting off sites of preferential attachment and thus removing the opportunity for denuded-zone formation.

B. *Ex situ* with 10–100 nm intermediate capping layers

In contrast to *in situ* experiments, *ex situ* FIB patterning could be masked by surface contamination. Despite thorough cleaning and an *in situ* anneal, contamination may still linger on the sample surface and dominate the island-nucleation processes. This is evidenced by the fact that transmission electron microscopists are frequently able to image small imperfections at the boundary between substrate and epilayers, regardless of the epigrowth technique. In our situation, lingering contaminants, picked up during transfer between buildings prior to insertion into the MBE, could mask the

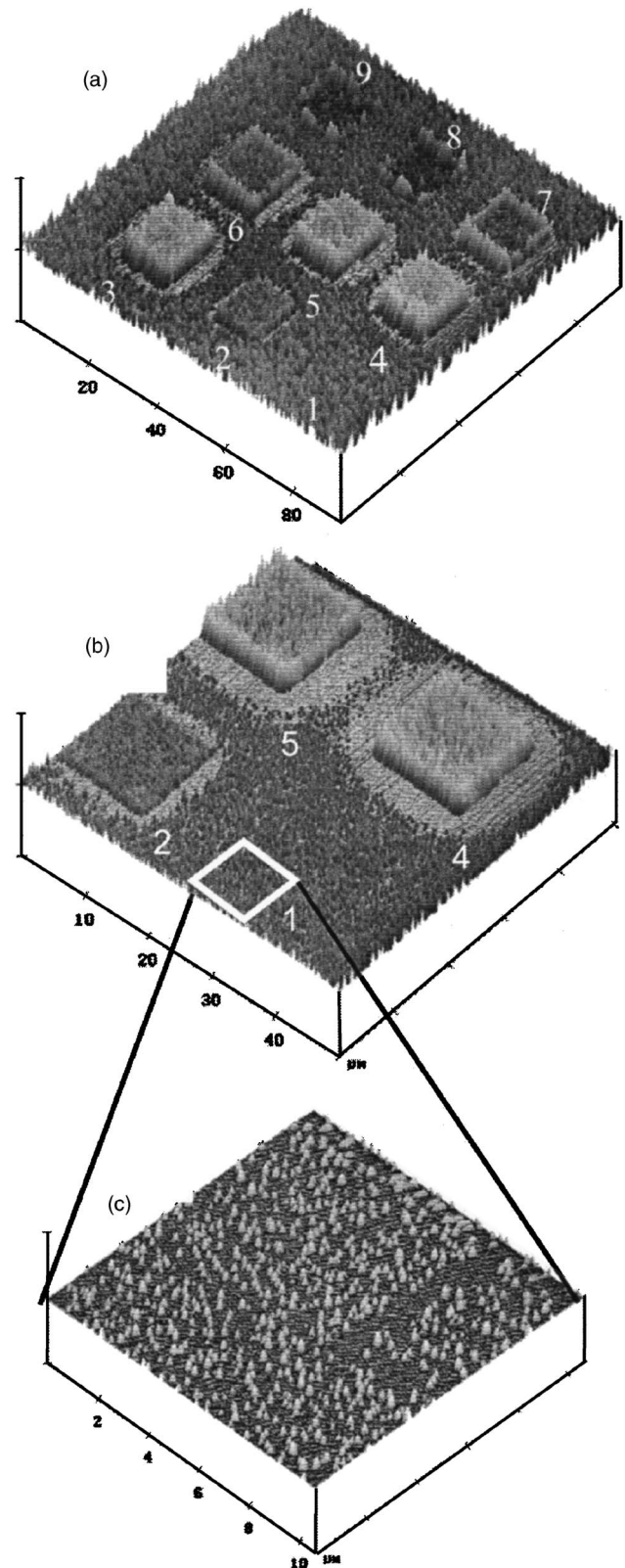


FIG. 5. (A) Matrix of nine implanted square areas, increasing in Ga dose. The dose-dependent effects ranged from no apparent alteration in the growth of subsequently deposited Ge (No. 1) to the milling of a depression (Nos. 5–9). (B) A magnification of the lower quadrant of (A), illustrating the growth of a denuded zone and increase in island size and number density. A very small dose of implanted Ga affects island nucleation. (C) A magnified scan of region No. 1, where a Ga⁺ dose of 2×10^{13} ions/cm² (0.04 ML) is just beginning to create a denuded zone.

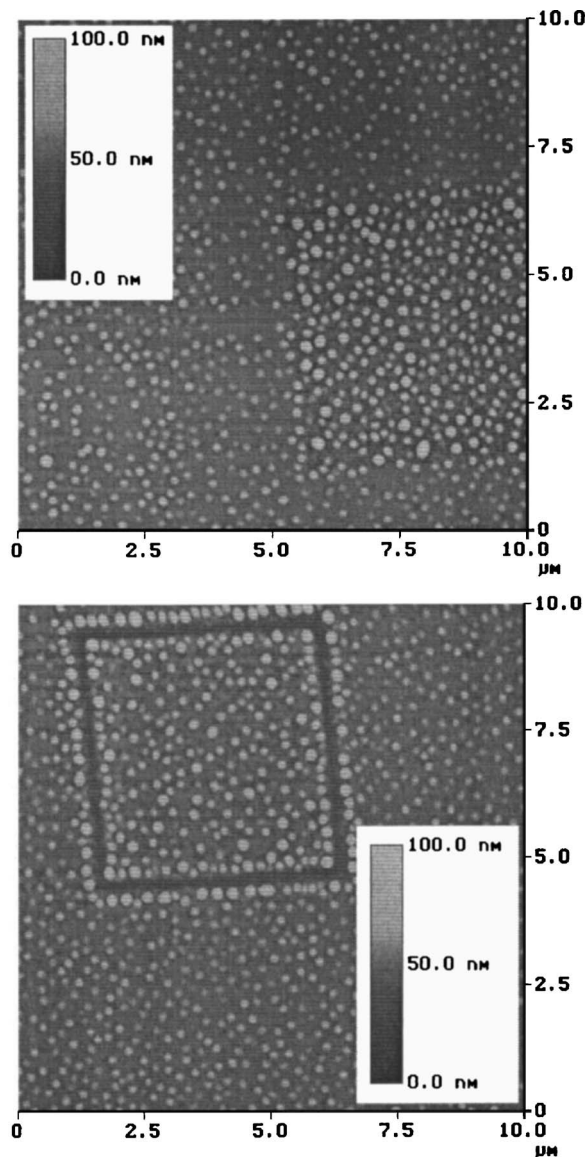


FIG. 6. At low doses, 7.5×10^{13} ions/cm² or 0.15 ML (upper) and 8.25×10^{14} ions/cm² or 1.65 ML (lower) and low capping layer thickness (10 nm), *ex situ* FIB-modification experiments produce similar results with respect to Ge nucleation to *in situ* FIB-modification growths

effect of the *ex situ* FIB patterning. To avoid this problem, a thin Si layer was applied in the MBE chamber over the FIB-patterned surface prior to Ge growth in order to bury the contaminants. With burial of the FIB-modified layer, patterning effects could be lost. To investigate this possibility, we performed a series of growths under *ex situ* conditions with capping layer thicknesses of 10, 30, and 100 nm. As shown in Fig. 6, results obtained at a capping layer thickness of 10 nm mirrored that observed for in the *in situ* studies. The Ga⁺-modified $5 \times 5 \mu\text{m}^2$ region, even at the lowest Ga⁺ dose (7.5×10^{13} ions/cm² or 0.15 ML) for which no topography was apparent, was distinguishable from the rest of the sample in two ways. First, the affected region had a greater density of larger dots (250–300 nm in diameter inside versus 220 nm outside). Second, the interisland surface in the implanted regions appeared slightly rougher than that in the

nonimplanted regions. At a higher Ga⁺ dose (8.25×10^{14} ions/cm² or 1.65 ML), we observed a row of islands bordering the implanted region. At a Ga⁺ dose of 8.75×10^{15} ions/cm² (17.5 ML), denuded zones formed beyond the bordering islands and surrounded the implanted regions. As Ga⁺ dosage increased, these denuded zones became narrower.

For samples with thicker capping layers (30 and 100 nm), growth modification was not observed at doses below 8.25×10^{14} ions/cm² (1.65 ML). In contrast, Ga⁺ doses of 3.57×10^{15} ions/cm² (7.14 ML) were sufficient to cause morphological changes for all capping layer thicknesses (Fig. 7). FIB-modified regions demonstrated larger islands for capping layers of both 10 and 30 nm thicknesses. For a capping layer of 100 nm, large clustered islands and significant pitting mark the implanted region. This phenomenon was also seen for 10 and 30 nm capping layers at higher Ga⁺ doses. Pitting and clustering of islands were not observed at the highest doses (1.05×10^{17} ions/cm² or 210 ML); instead, a low density of islands is observed in the implanted region (Fig. 8).

In the *ex situ* patterned samples, surface morphology adjacent to implanted regions was also strongly affected by Ga⁺ dose and capping layer thickness. For thicker capping layers, denuded zones appeared at lower doses. We believe that this occurs because of the surfactant nature of Ga, which allows it to float atop deposited Si and then diffuse outward from the center of the milled region. This increases the affected area and the concentration of Ga just beyond the borders of the implanted region, allowing for the formation of denuded zones at lower doses. Figure 7 shows a prominent denuded region for a 100 nm capping layer thickness at a dose of 3.57×10^{15} ions/cm² (7.14 ML). Following their initial appearance, the denuded zones follow a trend similar to that observed for a 10 nm capping thickness, decreasing in size with increasing Ga⁺. All higher Ga⁺ doses resulted in the formation of large islands bordering the implanted regions. Figure 9 summarizes all of the above *ex situ* results into one table: low-dose Ga⁺ effects disappear for capping layers thicker than 10 nm; for thicker capping layers, denuded zones form at a wider array of Ga doses; islands ring the implanted region for Ga⁺ doses larger than 8.25×10^{14} ions/cm².

IV. SUMMARY

We have shown that Ga⁺ doses into Si (100) as low as 2×10^{13} ions/cm² (equivalent to $\sim 1/100$ th of a monolayer) affect subsequent Ge epitaxial island nucleation. Thus, large scale guided islanding can be produced by brief milling, making this a potentially practical technology. For *in situ* FIB-based experiments, as Ga⁺ dose increased, the size of the denuded zone around the implanted region increased until significant milling occurred. This milling resulted in the formation of a cliff that separated the implanted region from the rest of the wafer, thereby acting as a barrier to adatom diffusion. As the pit deepened, the strength of the barrier increased, thus decreasing access to the preferential attach-

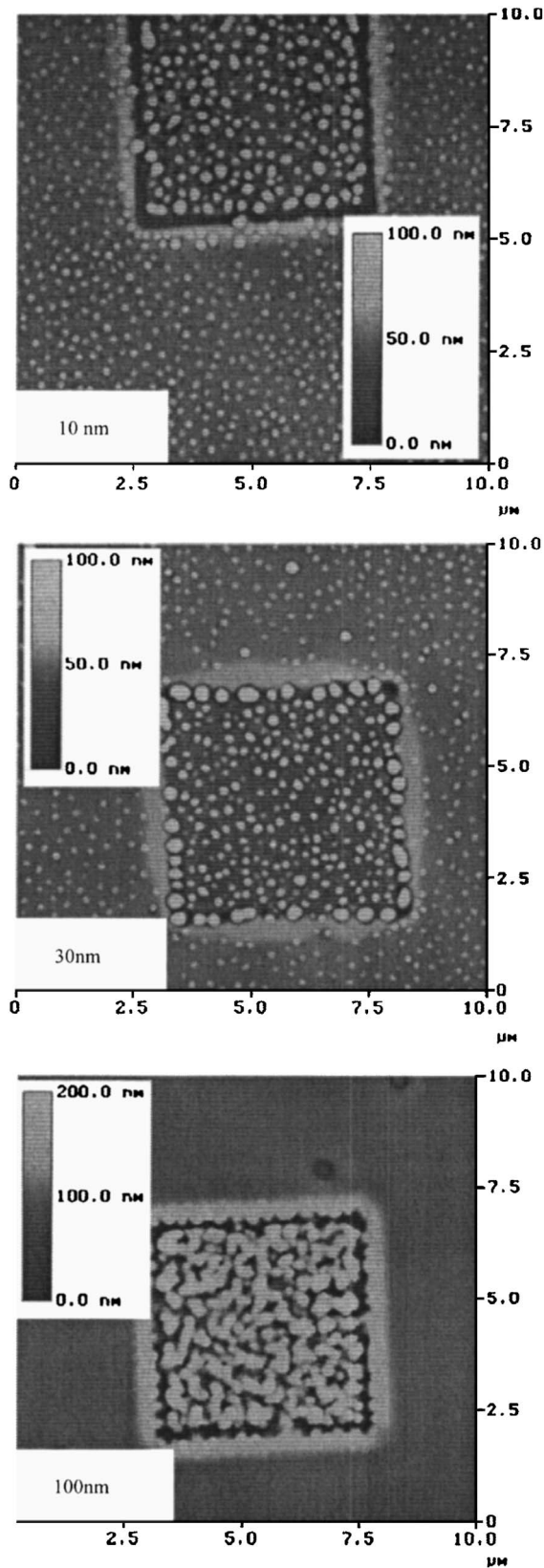


FIG. 7. Increasing capping layer thicknesses for a midlevel dose, 3.57×10^{15} ions/cm² (7.14 ML). Higher Ga-dose samples with a 10 nm capping layer demonstrate similar results to those obtained in absence of a capping layer. As capping layer thickness increases to 30 nm, more significant morphological changes are observed. 100-nm-thick capping layers generate very different results from shallow capping layers, with the appearance of large denuded zones and significant changes in island formation.

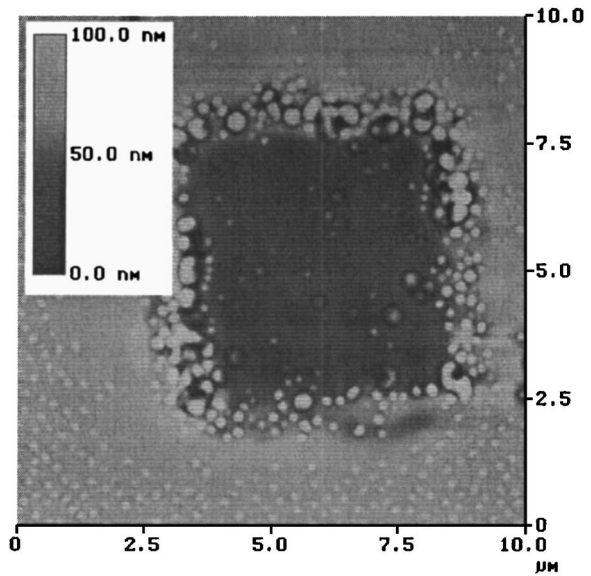


FIG. 8. Samples with thick capping layers continue to form denuded zones and islands in the patterned region even at high Ga doses. Growth conditions: $T=750$ °C, capping layer thickness=100 nm, Ga dose= 1.05×10^{17} ions/cm² (210 ML).

ment sites inside the implanted region, and the denuded zone therefore shrunk. Islands in the implanted region, especially along the edges, increased in size and number density with increased Ga⁺ dose. This trend continued until significant milling occurred and islanding ceased, instead being replaced by large scale roughness in the implanted region.

For the *ex situ* FIB-based experiments, the same effects were observed when we added a thin capping layer (10 nm). As the capping layer thickness increased, however, the observed effect varied more widely. For example, low-dose effects completely disappeared above 10 nm. Thicker capping layers produced in a denuded-zone formation under a wider

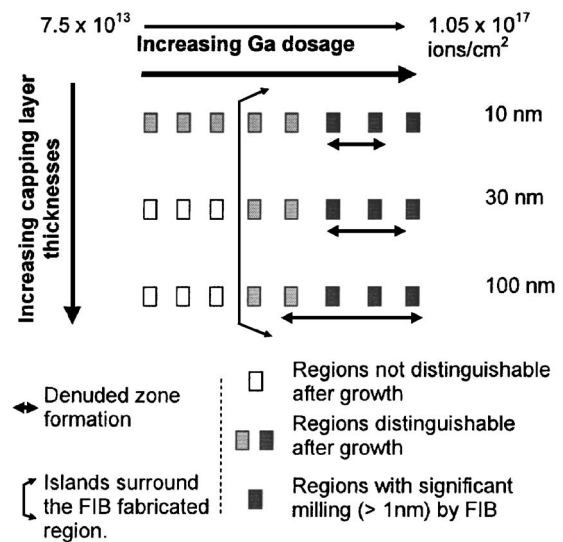


FIG. 9. Graphical summary of the results obtained for the *ex situ* variable-dose study. For all the samples above, the growth temperature was 750 °C and Ge-film thickness was 10 ML.

array of Ga⁺ doses and islands were found to ring the implanted region at Ga⁺ doses greater than 8.25×10^{14} ions/cm² (1.65 ML).

These light dose experiments are currently being expanded by our group to guide the growth of features in lines or at a single point. The increased diffusion length in the immediate patterned area allows for a larger collection area for the nucleated structures. This in turn allows structures to appear and evolve faster than in surrounding regions, creating hut clusters while the rest of the surface is flat.

In this article, we have examined a rapid preprocessing technique for guiding growth of quantum-dot islands. This technique may provide the basis for the creation of quantum-dot-based architectures with high feature densities and minimal patterning times, suggesting their potential commercial viability. These results imply that guided nucleation of Ge islands on Si by Ga⁺ focused ion beams, whether *in situ* or *ex situ*, is a versatile technique that offers great potential for realizing technological applications for quantum dots.

ACKNOWLEDGMENTS

This work was funded by NSF-DMR through the NSF-MRSEC at UVa, "The Center for Nanoscopic Materials Design."

¹W. K. Liu and M. B. Santos, *Thin Films: Heteroepitaxial Systems* (World Scientific, Singapore, 1999), Chap. 1.1.2.

²W. K. Liu and M. B. Santos, *Thin Films: Heteroepitaxial Systems* (World Scientific, Singapore, 1999), Chap. 2.

³J. P. Dismukes, L. Ekstrom, and R. J. Paff, *J. Phys. Chem.* **68**, 3021 (1964).

⁴R. Hull and J. C. Bean, *J. Vac. Sci. Technol. A* **7**, 2580 (1989).

⁵A. Braun, K. M. Briggs, and P. Böni, *J. Cryst. Growth* **241**, 1 (2002).

⁶E. Kasper, *Appl. Surf. Sci.* **102**, 189 (1996).

⁷R. People and J. C. Bean, *Appl. Phys. Lett.* **47**, 322 (1985); **49**, 229 (1986).

⁸R. M. Tromp and F. Ross, *Annu. Rev. Mater. Sci.* **30**, 431 (2000).

⁹R. M. Tromp, F. Ross, and M. C. Reuter, *Phys. Rev. Lett.* **84**, 4641 (2000).

¹⁰Y. W. Mo, D. E. Savage, B. S. Swartzentruber, and M. G. Lagally, *Phys. Rev. Lett.* **65**, 1020 (1990).

¹¹J. A. Floro, E. Chason, L. B. Frcund, R. D. Twisten, R. Q. Hwang, and G. A. Lucadamo, *Phys. Rev. B* **59**, 1990 (1999).

¹²M. Tomitori, K. Watanabe, M. Kobayashi, and O. Nishikawa, *Appl. Surf. Sci.* **76/77**, 322 (1994).

¹³G. Medeiros-Ribeiro, A. M. Bratkovski, T. I. Kamins, D. A. A. Ohlberg, and R. Stanley Williams, *Science* **279**, 353 (1998).

¹⁴F. M. Ross, J. Tersoff, and R. M. Tromp, *Phys. Rev. Lett.* **80**, 984 (1998).

¹⁵L. Jacak, P. Hawrylak, and A. Wójs, *Quantum Dots* (Springer, Berlin, 1998).

¹⁶T. I. Kamins, D. A. A. Ohlberg, R. Stanley Williams, W. Zhang, and S. Y. Chou, *Appl. Phys. Lett.* **74**, 1773 (1999).

¹⁷L. Vescan, T. Stoica, and B. Holländer, *Mater. Sci. Eng., B* **89**, 49 (2002).

¹⁸G. Jin, J. L. Liu, Y. H. Luo, and K. L. Wang, *Thin Solid Films* **369**, 49 (2000).

¹⁹M. Katayama, T. Nakayama, M. Aono, and C. F. McConville, *Phys. Rev. B* **54**, 8600 (1996).

²⁰A. Portavoce, F. Volpi, A. Ronda, P. Gas, and I. Berbezier, *Thin Solid Films* **380**, 164 (2000).

²¹X. W. Lin, Z. Liliental-Weber, J. Washburn, E. R. Weber, A. Sasaki, A. Wakahara, and T. Hasegawa, *Phys. Rev. B* **52**, 16581 (1995).

²²X. Zhou, B. Shi, Z. Jiang, W. Jiang, D. Hu, D. Gong, Y. Fan, X. Zhang, X. Wang, and Y. Li, *Thin Solid Films* **369**, 92 (2000).

²³H. Takamiya, M. Miura, N. Usami, T. Hattori, and Y. Shiraki, *Thin Solid Films* **369**, 84 (2000).

²⁴Y. Wakayama, G. Gerth, P. Werner, U. Gösele, and L. V. Sokolov, *J. Cryst. Growth* **231** 474 (2001).

²⁵M. Kammler, R. Hull, M. C. Reuter, and F. M. Ross, *Appl. Phys. Lett.* **82**, 1093 (2003).

²⁶J. B. Wang, A. Datta, and Y. L. Wang, *Appl. Surf. Sci.* **135** 129 (1998).

²⁷C. Lehrer, L. Frey, S. Petersen, and H. Ryssel, *J. Vac. Sci. Technol. B* **19**, 2533 (2001).